Review of Palaeobotany and Palynology 304 (2022) 104720

Contents lists available at ScienceDirect

Review of Palaeobotany and Palynology

journal homepage: www.elsevier.com/locate/revpalbo

Tissue decay tested in modern *Metasequoia* leaves: Implications for early diagenesis of leaves in fossil *Lagerstätten*

Caitlyn R. Witkowski [a,*,1], Qin Leng [a], Christopher W. Reid [a], Liang Feng [b], Hong Yang [a,*]

[a] Department of Science and Technology, Bryant University, 1150 Douglas Pike, Smithfield, RI 02917, USA
[b] Department of Microbiology, China University of Geosciences, 388 Lumo Rd, Hongshan, Wuhan, Hubei, PR China

ARTICLE INFO

Article history:
Received 27 April 2022
Received in revised form 22 June 2022
Accepted 27 June 2022
Available online 30 June 2022

Keywords:
Lagerstätte
Metasequoia
Early diagenesis
Morphology
Organic geochemistry

ABSTRACT

Sedimentary deposits yielding extraordinarily-preserved fossils (known as *Lagerstätten*) may provide significant insights into the physiology and environments of ancient plants, particularly when the fossils represent their original characteristics with limited diagenetic modifications. To better understand molecular, isotopic, and morphological changes during the early stages of diagenesis, degradation experiments were conducted in two time series: 1) a laboratory decay series using fungi on leaves over the course of a month and 2) a natural decay series with leaves collected from different stages of leaf senescence and early diagenesis. Both experiments used modern leaves of the dawn redwood *Metasequoia glyptostroboides*, referred to as a "living fossil" due to the morphological stability of the genus *Metasequoia* over the past 100 million years. Both decay series demonstrate that microbial degradation of polysaccharides occurs on extremely short timescales and results in cell collapse, first in the exclusively cellulose-based primary cell walls and then much later in the lignin-strengthened secondary cell walls. Despite morphological and molecular changes, the stable carbon isotopic composition of bulk leaves and *n*-alkanes remained virtually unchanged. Together, these findings suggest that: 1) rapid burial and tissue stabilization is essential in the formation of *Lagerstätte* fossils, 2) polysaccharides play a key role in maintaining three-dimensional fossil leaf structures and thus polysaccharide preservation implies rapid burial and minimal microbial degradation, and 3) carbon isotope signals, including at the molecular level, altered little during diagenesis. Thus, interpretations of physiological and environmental signals from conifer leaves in *Lagerstätten* are not likely impacted by early diagenesis.

1. Introduction

Sedimentary deposits yielding three-dimensionally-preserved plant fossils (known as *Lagerstätten*) provide key insights into plant systematics, physiology, and evolution, as well as reflecting the environment and climate under which those plants had grown. Based on the complex but predictable relationship that plants have with their environment, morphological information from *Lagerstätte* leaves can help reconstruct paleoclimatic parameters; for example, leaf shape reflects mean temperature and precipitation (e.g., Spicer et al., 2021; Butrim and Royer, 2020) and leaf stomata can reflect the atmospheric concentration of carbon dioxide (pCO_2) (e.g., Woodward, 1987; Barclay and Wing, 2016). Molecular and stable isotopic information from *Lagerstätte* leaves likewise reflect their growing environment; for example, the stable hydrogen isotopic composition of *Lagerstätte* leaves reflects the water the plant used during its life, thus informing us about regional hydrological cycles (Chikaraishi and Naraoka, 2003; Pagani et al., 2006; Polissar et al., 2009; Yang et al., 2009), and the stable carbon isotopic compositions of *Lagerstätte* leaves may reflect pCO_2 based on the isotopic fractionation that occurs during photosynthetic CO_2-fixation in plants (e.g., Cui and Schubert, 2016; Franks et al., 2014; Liang et al., 2022). These techniques have been developed over decades, improving the efficacy of leaf fossils as paleoenvironmental indicators.

Despite the utility of palaeobotanical proxies for reconstructing past environments, it is often difficult to distinguish whether these morphological, molecular, and isotopic features in leaf fossils represent the original physiological characteristics and environmental conditions or instead are expressing some modifications due to degradation and diagenesis of the fossil leaf tissues (Yang et al., 2005, 2007). High fidelity samples from Cenozoic plant fossil *Lagerstätten* have been reported, but the mechanism leading to their three-dimensional preservation remains poorly understood (Yang et al., 2005; Gupta et al., 2009; Leng

* Corresponding authors.
E-mail addresses: caitlyn.witkowski@bristol.ac.uk (C.R. Witkowski), hyang@bryant.edu (H. Yang).
[1] Present address: Schools of Chemistry and Earth Sciences, and Cabot Institute, University of Bristol, Bristol BS8 1TS, UK.

https://doi.org/10.1016/j.revpalbo.2022.104720

et al., 2010; Witkowski et al., 2012; Wang, 2010). A better understanding of this mechanism is key to evaluating the potential and limitations of the information provided by these well-preserved plant fossils (Liang et al., 2003; Briggs, 2003).

Previous studies revealed high concentrations of polysaccharides in morphologically well-preserved plant materials, leading to the hypothesis that polysaccharides play a key role in preserving the three-dimensional structures observed in *Lagerstätte* fossil plant cell walls (Yang, 2005; Yang et al., 2005, 2007; Gupta et al., 2009; Witkowski et al., 2012). To further test this hypothesis and to gain a better understanding of the early diagenesis process, we mimicked the process on *Metasequoia glyptostroboides* leaves in two decay series: a laboratory decay series under controlled condition by using polysaccharide-decomposing microbes and a natural decay series in an open pond environment. *M. glyptostroboides* was used because it is considered a model plant for comparing past and present environments given its morphological and genetic evolutionary stasis over the past 100 million years (Leng et al., 2001, 2010; Li and Yang, 2003a, 2003b; Yang and Jin, 2000; Yang et al., 2005, 2009). We also compared these two experimental studies on modern samples with exceptionally-preserved fossil *Metasequoia occidentalis* leaves from three Cenozoic fossil *Lagerstätten* in North America (Blanchette et al., 1991; McIver and Basinger, 1999; LePage et al., 2005; Yang et al., 2005).

In both decay series, biochemical and morphological methods were conducted in parallel in order to offer a mechanistic perspective. At each given time point, molecular analyses were conducted with pyrolysis-gas chromatography–mass spectrometry (py-GC-MS), polysaccharide concentrations are measured using UV–vis spectroscopy (UV–vis), bulk carbon isotopic values using isotope ratio mass spectrometry (IRMS), and the micromorphology was observed under a scanning electron microscope (SEM). To further understand the process and consequence of plant degradation, we compared the biochemical and morphological characteristics in our decayed modern samples with their fossil counterparts. With insights from these combined methodologies, we explored the biochemical basis of the observable three-dimensional preservation in Cenozoic *Lagerstätte* leaves and determine the fidelity of these remarkably well-preserved fossil leaves for environmental and climatic reconstructions.

2. Materials and methods

2.1. Metasequoia leaf samples

Three different sample sets of *Metasequoia* leaves were used for this study: 1) modern leaves for the laboratory decay series, 2) modern leaves for the natural decay series, and 3) fossil leaves from three Cenozoic localities (Table 1).

For the laboratory decay series, fresh green leaves from a mature *Metasequoia glyptostroboides* tree were collected from China University of Geosciences (CUG), Wuhan, Hubei Province, China (30°31′15.54″N, 114°23′59.16″E) during September 2011. All samples were taken from matured leafy branchlets at the same height (approximately 7 m) from the middle portion of branches. Leafy branchlets were cleaned with de-ionized water, and freeze-dried before storing at −80 °C prior to the experiment, leaves were open-exposed under an ultraviolet hood for 4 h of sterilization, with the upper and lower surfaces turned over every 30 min. All glassware used in the experiment was autoclaved, and all metal tools were cleaned with dichloromethane (DCM).

For the natural decay series, various stages of leaf senescence and tissue decay were collected from summer through winter of 2004 from the sole *M. glyptostroboides* tree in the Mt. Auburn Cemetery, Massachusetts, USA (42°22′21″N, 71°08′33″W). Details of these natural decay conditions were described in Gupta et al. (2009). Briefly, samples M-M-83-B1 through B3 were collected from the south side of the tree, representing green (M-M-83-B1), onset of color change (M-M-83-B2), and orange-red (M-M-83-B3) leaves. M-M-83-B4 samples were collected from the ground directly beneath the tree. From the small pond next to the tree, an environmental dredge was used to first collect that current year's (2004) fallen leaves at the water–sediment interface (M-M-83-B5) and used a second time to collect lake sediments presumably representing deposition from previous years (M-M-83-B6). Samples were stored at −80 °C after collection.

Table 1
Metasequoia leaf samples used in this study. Note 1: Abbreviations for locations (Loc.): AHI—Axel Heiberg Island, Arctic, Canada; CL—Clarkia, Idaho, USA; EI—Ellesmere Island, Arctic, Canada; MA—Mt Auburn Cemetery, Massachusetts, USA; WH—Wuhan, Hubei, China.

Sample no.	Age	Loc.	Type	Description
Clarkia	Miocene	CL	Fossil	
M-E-10	Eocene	AHI	Fossil	
M-E-10R	Eocene	AHI	Fossil	
M-P-15	Paleocene	EI	Fossil	
M-P-15R	Paleocene	EI	Fossil	
M-M-83-B1	Modern	MA	Natural	Green leaves from tree
M-M-83-B2	Modern	MA	Natural	Early senescence from tree
M-M-83-B3	Modern	MA	Natural	Late senescence from tree
M-M-83-B4	Modern	MA	Natural	Ground beneath tree
M-M-83-B5	Modern	MA	Natural	Pond, at sediment–water interface
M-M-83-B6	Modern	MA	Natural	Pond, in deep sediments
Gc-D00	Modern	WH	Laboratory	*Geotrichum candidum*, Day 0
Gc-D04	Modern	WH	Laboratory	*Geotrichum candidum*, Day 4
Gc-D09	Modern	WH	Laboratory	*Geotrichum candidum*, Day 9
Gc-D21	Modern	WH	Laboratory	*Geotrichum candidum*, Day 21
Gc-D25	Modern	WH	Laboratory	*Geotrichum candidum*, Day 25

The following *M. occidentalis* fossil leaves from three Cenozoic localities were used for comparison with modern samples: 1) M-P-15 samples were collected from the lignite beds at the top of Member 2 of the Iceberg Bay Formation at Stenkul Fiord, Ellesmere Island, Canadian Arctic Archipelago (77°20′58″N, 83°26′08″W). The fossil-bearing late Paleocene sediments were dated as ca. 60 Ma in age (Yang et al., 2005). 2) M-E-10 samples were collected from the Upper Coal Member in the Buchanan Lake Formation at Axel Heiberg Island, Canadian Arctic Archipelago (79°54′55.8″N, 89°01′26.8″W). The member was dated as 41.3–47.5 Ma (middle Eocene) (Eberle and Storer 1999). 3) M-C-11 samples were collected from the UIMM P-33 Clarkia fossil site near Clarkia, Idaho, USA (46°59′29.3″N, 116°16′35.8″W). This middle Miocene was recently dated as 15.78 ± 0.039 Ma (Höfig et al., 2021). Detailed descriptions of these fossil samples, as well as their geological settings, were previously published in Yang et al. (2005).

2.2. Microbial strains for laboratory degradation

Polysaccharide-degrading microbes were introduced to modern leaves under controlled conditions in the laboratory degradation experiment. Pure fungal (ascomycete) species *Geotrichum candidum* were grown in sterile media consisting of NH_4Cl (0.1% m/v), Na_2HPO_4 (1% m/v), $KHPO_4$ (0.15% m/v), levoglucosan (0.2% m/v), agar (2%), $MgSO_4$ (0.1% m/v), and $CaCl_2$ (5% m/v) in 50 mL of water. The cultures were independently introduced to four sets of petri dishes containing *M. glyptostroboides* leaves. A concentration of 0.5 mL of each culture (with 1 M NH_3NO_3 solution as a nitrogen source) was added to 1 g of leaves. These experimental sets were placed in a 30 °C incubator to optimize microbial growth. Once a week, samples were supplied with 1 mL of autoclaved tap water. Every four to five days, three petri dishes from each set were removed from the incubator and placed into a freezer at −20 °C to terminate microbial growth. The experiment was carried out for a period of 25 d in triplicate.

2.3. Py-GC-MS analyses

Crushed samples (2 mg each) were manually extracted three times via ultrasonication using DCM:MeOH (2:1 *v*/*v*) for 15 min each (Yang et al., 2005; Witkowski et al., 2012). After samples were dried, precisely 0.5 mg of the remaining sample was placed in a thermally-sterilized

quartz tube with glass wool and inserted into a CDS 1500 pyroprobe with an interface of 250 °C. The probe was set at 610 °C for 15 s in a flow of helium gas. Agilent 7890A GC with a silica capillary column (30 m × 250 μm, 0.25 μm film thickness) was used with helium as the carrier gas. The GC oven was held at 40 °C for 5 min isothermal to 100 °C at a rate of 10 °C/min, and then increased to 300 °C at a rate of 10 °C/min. Agilent 5975C Series GCMSD MS was operated in full scan mode at 70 eV (Yang et al., 2005; Gupta et al., 2009; Witkowski et al., 2012). Peaks were identified via the NIST mass spectral library and other references (Pouwels et al., 1989; van Bergen et al., 1996; Yang et al., 2005; Witkowski et al., 2012).

2.4. Reducing sugar assay

Polysaccharide content of *M. glyptostroboides* leaf samples was determined using the 3-methyl-2-benzothiazolinone hydrazone (MBTH) assay described by Anthon and Barrett (2001) with the addition of hydrolysis (Opsahl and Benner, 1999). Briefly, 10 mg of crushed sample were pretreated with 100 μL of 12 M H_2SO_4 for 2 h and then diluted to 1.2 M and hydrolyzed for 3 h at 95 °C. Samples were diluted to 1:100 (with double-distilled H_2O) and were mixed with 0.5 M NaOH and 40 μL MBTH reagent (equal volumes of 3 mg/mL MBTH and 1 mg/mL DTT). Samples were heated at 80 °C for 15 min, followed by the addition of 80 μL of a solution containing $(FeNH_4(SO_4)_2) \cdot 12H_2O$, 0.5% (*v*/*v*) H_2SO_4, and 0.25 M HCl. Reducing sugar content was measured using Molecular Devices Spectra Max 190 with SoftMax software package at a wavelength of 620 nm. Assay response was calibrated using the monosaccharides of D-glucose and a *N*-acetylglucosamine as standards, respectively. Results reported in mol reducing sugar/g plant cell mass (mol/g). All samples were run in triplicate.

2.5. $\delta^{13}C$ of bulk leaf tissues and n-alkanes

The stable carbon isotopic composition ($\delta^{13}C$) of the bulk leaf for the laboratory decay series were measured using offline IRMS at the State Key Laboratory of Loess and Quaternary Geology, Institute of Earth Environment, Chinese Academy of Sciences in Xi'an, Shaanxi Province, China, following standard carbon isotope measurement protocols (Yang et al., 2011). Samples were first air-dried and crushed, then evacuated for 1 h at 800 °C, and sealed in the presence of CuO, Cu foil, and Ag foil. Cryogenic distillation purified and isolated the trapped CO_2, which was then measured using a MAT-251 offline gas mass spectrometer with a dual inlet system (Liu et al., 2005). The standard analytical error was less than 0.3‰. All samples were run in triplicate.

The $\delta^{13}C$ of bulk leaf tissue and *n*-alkanes from the natural decay series and from fossil *Metasequoia* were measured using an online IRMS system at the Earth System Center for Stable Isotopic Studies (ESCSIS) of Yale University. Air-dried and crushed samples were placed into 4 × 6 mm silver capsules, which were combusted for bulk isotope measurements on a Costech ECS 4010 EA elemental analyzer connected to a ThermoFinnigan DeltaPlus Advantage IRMS at the ESCSIS (Yang et al., 2011). The ESCSIS working standard was a house Cocoa ($\delta^{13}C = -28.42$‰, 48.7% C). The standard deviations of replicate samples are 0.05‰. Total lipid extraction was carried out with a Dionex 300 Accelerated Solvent Extractor five times at 125 °C, 1500 p.s.i. for 25-min using dichloromethane (DCM):methanol = 2:1(*v*/*v*) buffer. Solid phase ion exchange columns (70–230 mesh) were used to separate free carboxylic acids from the neutral lipid fractions, which were further purified to obtain *n*-alkanes by silica gel flash column chromatography (Yang and Huang, 2003). Concentrations of the individual compounds were determined using HP6890 gas chromatograph mass spectrometry (GC/MS) using a DB-1 capillary column (60 m X 0.25 mm X 0.25 μm). The $\delta^{13}C$ values of individual lipid compounds were determined by isotope ratio monitoring-gas chromatography/thermal conversion/mass spectrometry (irm-GC/TC/MS) using a Thermo Finnigan MAT 253 mass spectrometer interfaced with a Thermo Finnigan high temperature conversion system. The analytical instrumentation error was ±0.5‰ or better. All $\delta^{13}C$ values are expressed relative to the VPDB standard defined as: $\delta^{13}C = 1000 \times [(^{13}C/^{12}C_{sample})/(^{13}C/^{12}C_{VPDB}) - 1]$. All samples were run in triplicate.

2.6. SEM observations

A JEOL JSM-6010LA SEM was used to document morphological changes of leaf cells, mainly their cell walls. A 1 mm long transverse section was cut using a single-edged razor blade from the middle portion of a leaf located at the middle portion on the branchlet for a standardized comparison because micromorphological features of different leaf parts (from leaf base to apex) as well as of leaves located in different places on leafy branchlet, branch, and tree can vary drastically in *M. glyptostroboides* (Wang, 2010; Liang et al., 2022). The sections were mounted on SEM stubs using double-sided tape with the cut surface facing upward and air-dried overnight. Mounted cuttings were sputter-coated with ca. 17.5 nm of gold by a Denton Desk V HP Cold-Sputter Coater and then observed via SEM at accelerating voltage of 8 or 10 kV. All cuttings were done in at least duplicate.

3. Results

3.1. Laboratory decay series

Levoglucosan and agar were the only carbohydrate sources in the medium. Levoglucosan was used because it is the most abundant polysaccharide pyrolysate in *Metasequoia* leaves (Yang et al., 2005, 2007; Gupta et al., 2009; Witkowski et al., 2012). Because different fungal species produce different enzymes committed to degrading specific polysaccharides (van den Brink and de Vries, 2011), laboratory experiments were first conducted to test the polysaccharide-degrading effectiveness of different fungal strains available in the Laboratory of Microbiology at CUG and its collaborative laboratories. Pure species *Geotrichum candidum* grew very quickly and were found to be effective in degrading levoglucosan. *G. candidum* was further chosen due to its global distribution and high abundance in soil and compost, air, and water. Bajpai et al. (2007) suggest that *Metasequoia* may have essential oils that impact some fungi, but appears to have not inhibited the growth observed here. The experiment was carried out for a period of 25 d in triplicate, long enough to mimic early stages of diagenesis.

3.2. Py-GC-MS

In the laboratory decay series, the Py-GC-MS analyses yielded expected pyrolysates for *Metasequoia* leaves (Yang et al., 2005, 2007; Gupta et al., 2009). Nine polysaccharide pyrolysates were semi-quantified: 2-methylfuran, acetic acid, 2-furaldehyde, 2-hydroxy-2-methyl-2-cyclopenten*e*-1-one, 5-methyl-2-furfuraldehyde, 4-hydroxy-5,6-dihydro (2H) pyra*n*-2-one, 3 hydroxy-2-methyl-(4H)-pyra*n*-4-one, and levoglucosan (Table 2). Levoglucosan, the most abundant and most stable polysaccharide pyrolysates found in *Metasequoia* leaves, is shown in Fig. 1a to illustrate the general trend among polysaccharide fragments throughout the laboratory decay series. There is a decrease in relative area from Day 0 samples at 20166, to Day 4 samples at 8349, to Day 9 at 5888. There is then a later increase in Day 21 samples at 9845 to finally Day 25 samples at 14105. Most polysaccharides trend similarly to levoglucosan, in which the amount decreases in the first several days and then later increases, ending the series just below the initial abundance of polysaccharides (Table 2).

Data on the relative compound areas for the natural decay series (Gupta et al., 2009) and the fossil samples (Yang et al., 2005) were previously published. Unlike results from the laboratory decay series, samples in natural decay series show a progressive decrease in polysaccharide concentration as indicated by Py-GC–MS data and C:N content (Gupta et al., 2009).

Table 2
Area of polysaccharide pyrolysates in *Geotrichum candidum*-induced laboratory decay series of *Metasequoia glyptostroboides* leaves from Day 0 through Day 25. Fragment ions (frag) for the compounds are based on the mass-to-charge ratios (m/z).

#	Compound name	Frag (m/z)	Day				
			0	4	9	21	25
1	2-methylfuran	82, 81, 53	2806	890	1411	890	2669
2	Acetic acid	60	3511	1454	2842	1540	3769
3	2-furaldehyde	96, 95, 39	2426	1192	1829	1066	3007
4	2-methyl-2-cyclopenten-one	98, 55, 69	3053	674	1214	1216	3138
5	5-methyl-2-furfuraldehyde	110, 53, 81	2407	718	1417	591	3056
6	4-hydroxy-5,6-dihydro (2H) pyran-2-one	114, 58	1127	754	957	343	666
7	2-hydroxy-3-methyl-2-cyclopenten-1-one	112, 55, 69	5225	705	1545	1110	4742
8	3 hydroxy-2-methyl-(4H)-pyran-4-one	126, 42, 71	1686	302	1149	1050	2873
9	Levoglucosan	60, 73	20,166	8349	5888	9845	14,105

3.3. Degradation of cell wall polysaccharides

Consistent with results from Py-GC–MS analysis, the MBTH sugar-reducing assay on laboratory decay series resulted in an initial decrease followed by an increase of polysaccharide abundances in later samples (Fig. 1b). A high initial sugar count of 0.6164 mol/g on Day 0 samples decreased to 0.4407 mol/g in Day 4 and then to 0.3843 mol/g in Day 9 samples. Day 21 at 0.5418 mol/g increased to 0.6101 in Day 25 samples, just below the initial starting value. Total reducing sugar content was determined for the three fossil samples. Fossil samples averaged 0.6180 mol/g fossil, approximately the same total reducing sugar abundance as observed in the Day 0 laboratory decay series.

3.4. $\delta^{13}C$ of bulk leaf tissue and n-alkanes

The *G. candidum*-induced laboratory decay series showed little change in the $\delta^{13}C$ of bulk leaves over the 25d period, ranging from −27.7 to −27.6‰ (Table 3 and Fig. 2). In the natural decay series, however, a slight negative offset in the $\delta^{13}C$ of bulk leaves was observed from M-M-83-B2 (−27.8‰) to M-M-83-B3 (−28.4‰), leaves still growing on the tree but representing early to late stages of senescence (Table 3 and Fig. 2). Partial data of $\delta^{13}C$ of lipid-free leaf residues were previously reported (Liang et al., 2022). No obvious $\delta^{13}C$ value changes were measured in the last four samples in the natural decay series, M-M-83-B3 through M-M-83-B6, all fallen leaves, although the last two samples have lower carbon concentrations, implying significant tissue loss during progressive decay (Table 3). The $\delta^{13}C$ values of dominant *n*-alkane compounds (chain-lengths C_{27}, C_{29}, and C_{31}) have similar mean averages and standard deviations (SD) throughout the natural decay series: respectively, −32.3‰ ± 0.6‰ SD for C_{27} *n*-alkane, −32.5‰ ± 0.3‰ SD for C_{29}, and − 32.5‰ ± 0.2‰ SD for C_{31} (Table 4; Fig. 3). All data across the natural decay series falls within 2SD of the mean (Table 4; Fig. 3), with the exception of one point which falls outside by 0.1‰ (highlighted in Table 4); however, this is negligible when considering that the accuracy of the analytical instrumentation encompasses a ± 0.5‰ error. Contrary to the modern samples, the fossil *Metasequoia* samples show enriched $\delta^{13}C$ values of approximately 4‰ more positive than their modern counterparts (Table 3; Table 4; Fig. 2). The $\delta^{13}C$ values of the bulk leaf tissues range from −24.5 to −23.7‰ and the $\delta^{13}C$ values of the dominant C_{27}, C_{29}, and C_{31} *n*-alkanes range from −27.4 to −28.7‰.

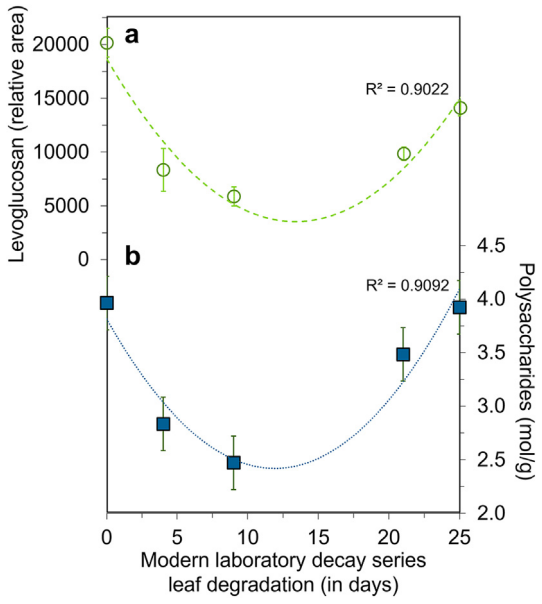

Fig. 1. Change in polysaccharide pyrolysate areas over 25 days in *Geotrichum candidum*-induced laboratory decay series of *Metasequoia glyptostroboides* leaves. a) Relative area of levoglucosan (Lv) in Py-GC–MS counts over time. b) Quantitative change in bulk polysaccharide in mol/g over time via MBTH assay. Error bars represent standard deviation of triplicate analytical runs for the triplicate experiments for each time point.

3.5. Morphological decay

SEM results show an obvious and continuous decay of three-dimensional structures within modern leaves (Plates I, II). As shown in Plate I, we observed the entire cross-section of the middle portion (mid-rib) of *Metasequoia* leaves throughout both the laboratory (Plate I, 1–4) and natural decay series (Plate I, 5–8). This provides visual access to the vascular bundle, the critical tissues that transport water (primarily via the xylem, the larger cells within the bundle that are closer to the upper surface) and transport nutrients (primarily via the phloem, the smaller cells closer to the lower surface). The vascular

Table 3
The $\delta^{13}C$ of bulk leaf tissue (‰) and weight percent carbon (wt%C) for fossil *Metasequoia occidentalis* and decay series *M. glyptostroboides* samples. See Table 1 for detailed sample names.

Sample no.	$\delta^{13}C$ (‰)	wt%C
M-E-10	−24.46	33.36
M-E-10R	−23.73	42.23
M-P-15	−24.53	34.82
M-P-15R	−24.40	33.04
M-M-83-B1	−27.88	49.90
M-M-83-B2	−27.78	47.43
M-M-83-B3	−28.40	48.17
M-M-83-B4	−28.25	50.67
M-M-83-B5	−28.20	34.20
M-M-83-B6	−28.45	39.07
Gc-D00	−27.62	
Gc-D04	−27.66	
Gc-D09	−27.66	
Gc-D21	−27.57	
Gc-D25	−27.58	

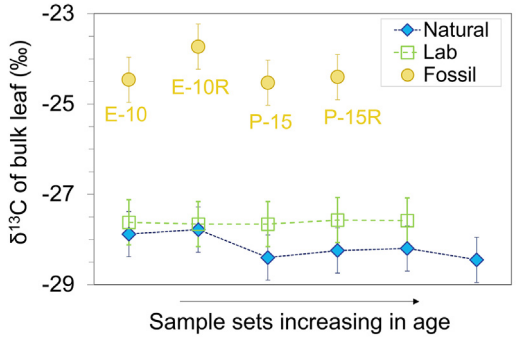

Fig. 2. Bulk leaf tissue $\delta^{13}C$ from *Metasequoia*. Natural decay series numbers (with increasing degradation from M-M-B83–1 through 6, blue diamonds) and laboratory decay series numbers (with increasing degradation from Day 0 through Day 25, green squares). Fossils (yellow circles) are labeled (see Table 1) in increasing age. Analytical instrument error is ±0.5 ‰.

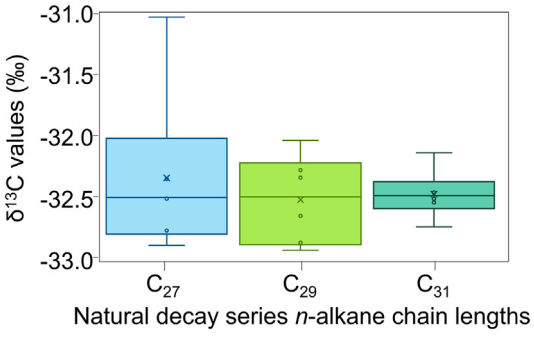

Fig. 3. The $\delta^{13}C$ of the dominant *n*-alkanes (chain-length C_{27}, C_{29}, C_{31}) in modern *Metasequoia glyptostroboides* leaves in the natural decay series (M-M-83-B1 through B6). Analytical instrument error is ±0.5 ‰.

bundle (and adjacent area including the transfusion tissues) are the most ideal places to observe the micromorphological changes; it is the only place within a *Metasequoia* leaf to have both cells that have only primary cell walls (cellulose- and hemicellulose-based) and cells that have both primary and secondary cell walls (lignin-strengthened), which we observe throughout the two decay series.

For the laboratory decay series, Plate I shows the degradation of the vascular bundle over time, from early in the series (Plate I, 1) through to the final day of the series (Plate I, 4). Plate II likewise shows "before and after" images throughout the degradation process, with examples of early degradation on the lefthand side of the plate (Plate II, 1–4) and latter degradation on the righthand side of the plate (Plate II, 5–8). At the start of the series, all the cells are expectedly intact, as seen in the overall leaf section including its margins (Plate II, 1), throughout the vascular bundle (center of Plate I, 1), and in a close-up of the xylem (center of Plate II, 2) which are three-dimensionally intact and rigid. All tracheids in the xylem and transfusion tissue show their unevenly deposited secondary walls, thin primary walls, and middle lamellae shared with neighboring cells in a consolidated pattern, as exemplified in the closeup on Plate II, 2. Day 4 samples display slight changes, mainly on parenchyma cells in the lateral areas of the leaf with no noticeable change seen in the vascular bundle (Plate I, 1) but no fungal hyphae are observed on or within the leaf (Plate II, 1).

The following days of the laboratory decay all show signs of degradation. On Day 9 samples, there are early signs of fungal growth, including fungal hyphae seen on the lower leaf surface. The fungal hyphae start to enter the leaf via the stomata (Plate II, 4), the only openings on the leaf cuticle membrane, and quickly grow and expand throughout the leaf, almost reaching the mid-vein on Day 9 (Plate I, 2). Some phloem cells start to collapse, while some lignin-strengthened secondary cell walls start to detach a little from the primary cell walls of the tracheids (Plate II, 3), although the tracheids still maintain their three-dimensional structures (Plate I, 2). Day 21 samples display obvious internal and external degradation and cell collapse (Plate I, 3; Plate II, 5) with the rapidly growing fungal hyphae seen throughout the leaf with severe intrusion through the stomata (Plate II, 8). Phloem cells are largely collapsed, with individual cells hardly recognizable (Plate I, 3). Tracheids are not as rigid as in previous samples; there is obvious detachment (Plate II, 6) and unraveling of the unevenly-deposited lignified secondary cell walls (Plate II, 7). Finally, Day 25 samples then show the complete infiltration of fungal hyphae, with their string-like bodies abundantly observable everywhere on and within the leaf. Their dominant occupation is directly correlative with the disappearing leaf cell walls; most cells, including those in the vascular bundle and transfusion tissue, are collapsed (Plate I, 4) and thus represents the end of the laboratory decay series.

For natural decay series samples, we observed their leaf cross sections under the same SEM observation conditions (Plate I, 5–8). Here, we show a selection of the samples throughout the natural decay series of early senescence (M-M-83-B2; Plate I, 5), late senescence (M-M-83-B3; Plate I, 6), at the water–sediment interface in the pond next to the tree (M-M-83-B5; Plate I, 7), and deeper into the pond sediments (M-M-83-B6; Plate I, 8). Samples M-M-83-B1 to B4 display no obvious micromorphological change. Degradation is seen in samples M-M-83-B5 and B6, the two samples collected from pond sediment. M-M-83B5 was the product of the 2004 collecting year, deposited for approximately one month and displays slight degree of degradation. M-M-83-B6, collected from sediments deeper in the lake, has presumably been decaying for at least one year and shows more extensive loss of cell wall material which caused the phloem cells collapsed and compressed.

4. Discussion

4.1. Changes in polysaccharide contents

We observed a decline of polysaccharides over time in our natural decay series and in the initial days (Day 0–9) of our laboratory decay series. This likely reflects the process common to leaf litter degradation, in which up to 50% of polysaccharides may be degraded via microbial processes prior to incorporation into sediment (Lallier-Vergès et al., 2008); for example, fungi produce exocellulase enzymes that decompose cellulose, generally by hydrolyzing the exposed β(1➔4) linkages in cellulose and related polysaccharides (Barr et al., 1996). As expected, the natural decay series shows a continually decrease in polysaccharide abundance

Table 4
The $\delta^{13}C$ in ‰ of the dominant *n*-alkanes (chain-length C_{27}, C_{29}, C_{31}) in modern *Metasequoia* in the natural decay series (M-M-83-B1 through B6), as well as the mean average, standard deviation (SD), and the two standard deviation range of each *n*-alkane chain-length across the natural decay series. The * symbol denotes values lying outside the two standard deviation range. Analytical instrument error is ±0.5 ‰.

n-alkane	B1	B2	B3	B4	B5	B6	Mean	SD	-2SD	+2SD
C27	−31.0*	−32.9	−32.5	−32.5	−32.8	−32.3	−32.3	0.6	−33.6	−31.1
C29	−32.6	−32.3	−32.9	−32.0	−32.3	−32.9	−32.5	0.3	−33.2	−31.9
C31	−32.5	−32.1	−32.5	−32.4	−32.7	−32.5	−32.5	0.2	−32.8	−32.1

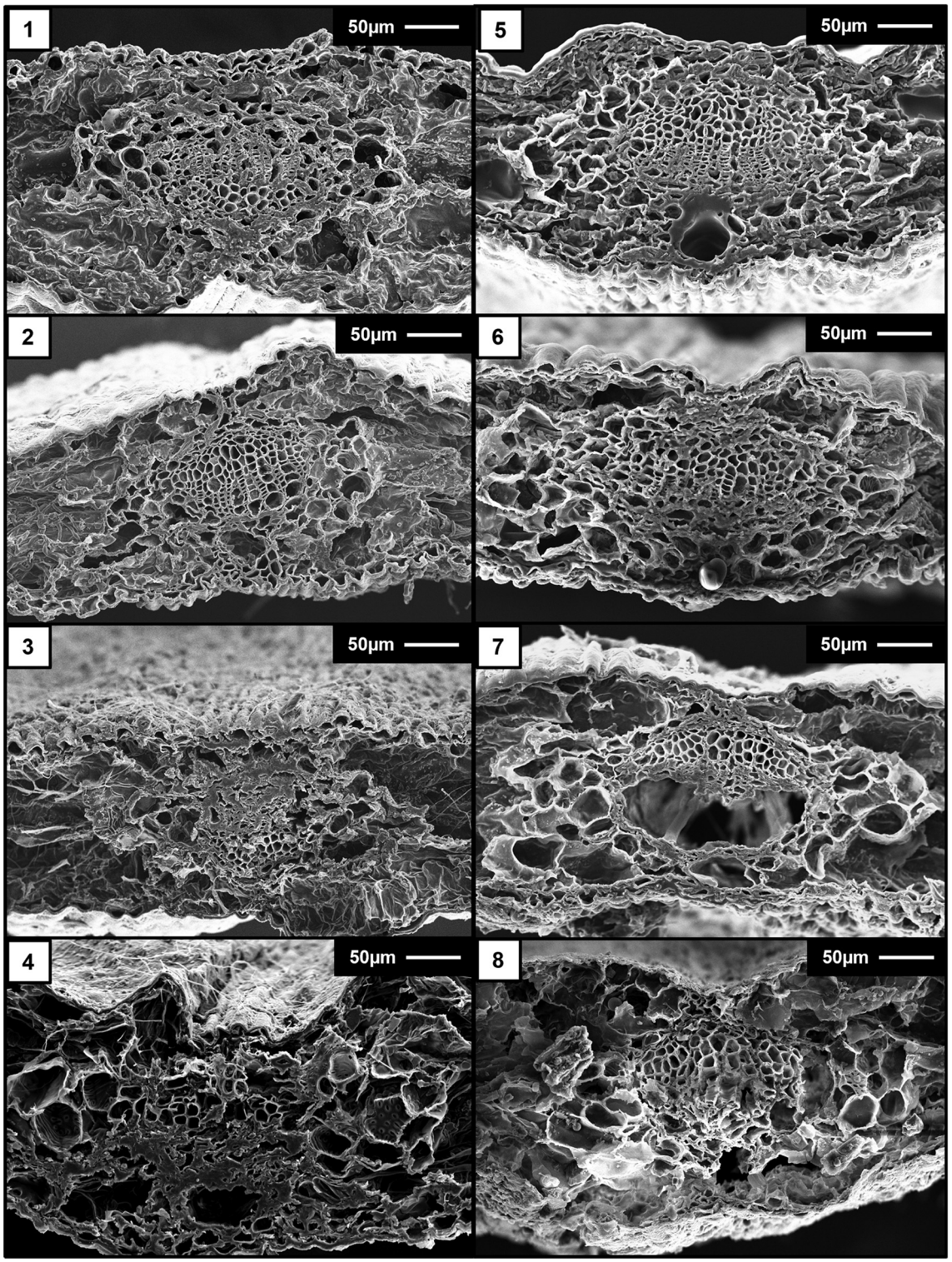

Plate I. SEM micrographs of *Metasequoia glyptostroboides* leaves in the laboratory decay series (figs. 1–4) and natural decay series (figs. 5–8). The selection of the laboratory decay series using *Geotrichum candidum* (GC) includes after 4 days (GC-04, fig. 1), 9 days (GC-09, fig. 2), 21 days (GC-21, fig. 3), and 25 days (GC-25, fig. 4). The selection of the natural decay series includes leaves from early senescence (M-M-83 B-2, fig. 5), late senescence (M-M-83 B-3, fig. 6), the pond surface (M-M-83 B-5, fig. 7), and deeper in the pond (M-M-83 B-6, fig. 8). All figures show the midrib in the center of the image with the adaxial (upper) surface of the leaf needle facing upward so that in the vascular bundle the xylem is above the phloem.

with progressive decay, including levoglucosan which decreases from sample M-M-83-B1 through B6 in parallel with morphological changes in decay (Gupta et al., 2009). As expected, the laboratory decay series also showed rapid decline in polysaccharides, as supported by ca. 48% decrease in overall polysaccharides (Fig. 1b) and ca. 70% decrease in levoglucosan (Fig. 1a). However, the total polysaccharide content then appears to increase halfway through the laboratory decay series (Fig. 1).

The laboratory decay series results were initially surprising given that the experiment was designed to mimic nature and was thus expected to behave similarly to the natural decay series, in which

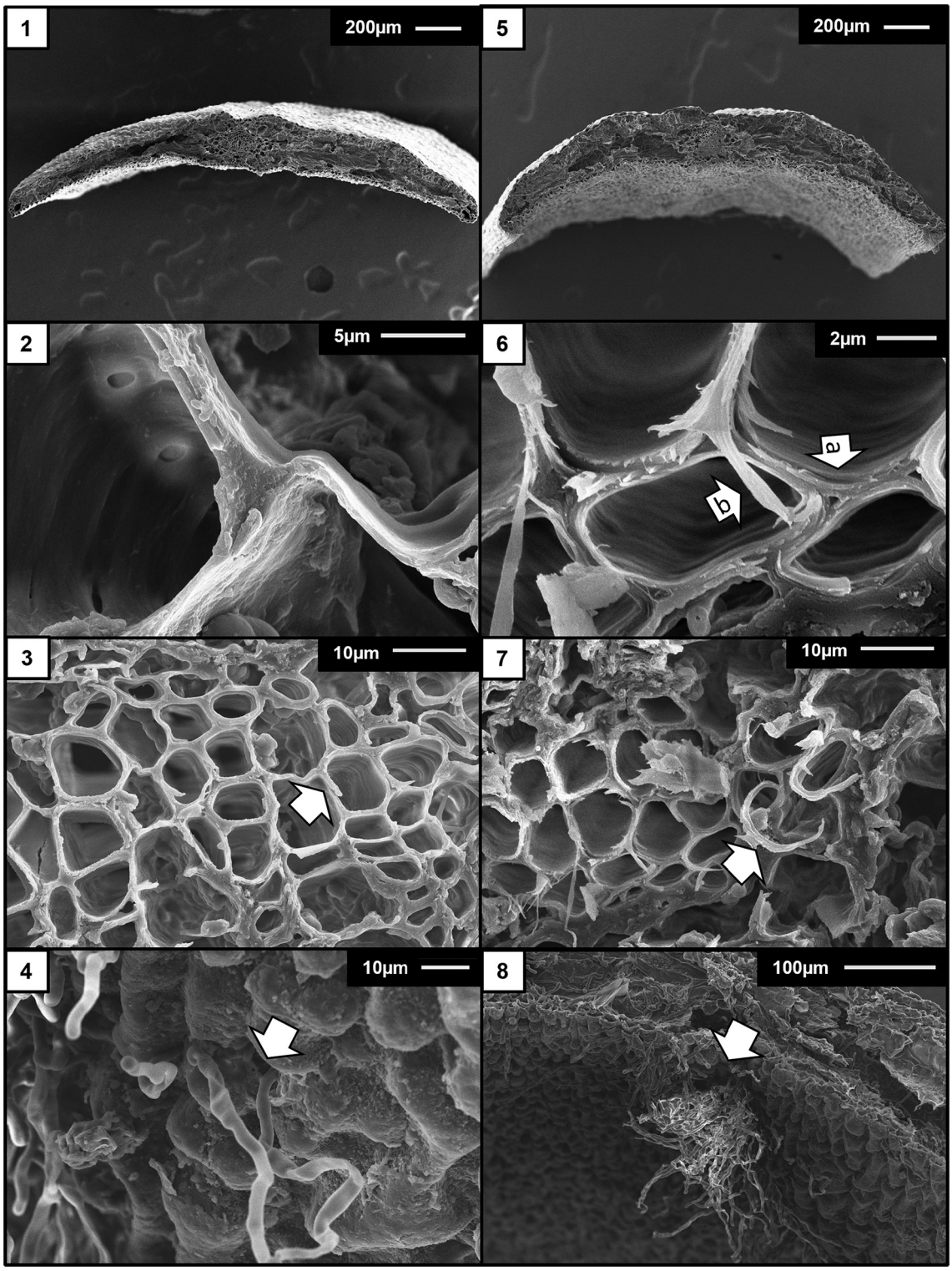

Plate II. SEM micrographs of *Metasequoia glyptostroboides* leaves in the laboratory decay series, demonstrating structural changes throughout the series with earlier days on the left ("before", figs. 1–4) and later days on the right ("after", figs. 5–8). An overview of the leaf section is shown for day 4 (fig. 1) where the hyphae are only starting to grow on the outer leaf and day 21 (fig. 5) where the hyphae have fully penetrated the inner leaf. A close-up of the xylem is shown for day 0 (fig. 2) with fully intact cell walls versus day 21 (fig. 6) where there is severe loss of the primary cell wall (arrow a) and partial detachment of the secondary cell wall (arrow b), shown peeling away. The onset of this cell wall loss begins in day 9 (fig. 3), as indicated by the white arrow, which then later results in the unraveling of the cell wall on day 21 (fig. 7) as indicated by the white arrow. Fungal hyphae penetration occurs through the leaf stomata on the abaxial leaf surface as indicated by the arrows, which appears to begin shortly before day 9 (fig. 4) and escalates to major intrusion by day 21 (fig. 8). All figures show the adaxial (upper) surface of the leaf needle facing upward so that in the vascular bundle the xylem is above the phloem.

polysaccharide contents decrease throughout the entire series. In the design of the laboratory decay series, fungi was chosen for its major role in the degradation of leaf litter, comprising up to ca. 67% of the microbial mass in leaf litter aboveground and up to ca. 99% of the microbial mass in leaf litter in streams (Wei et al., 2009), and this specific fungus *Geotrichum candidum* was chosen for its high abundance in natural

settings, including soil, compost, air, and water (Eliskases-Lechner et al., 2022). However, on further investigation, we noted that the increase in polysaccharide abundance from Day 9 to Day 21 samples (Fig. 1, Table 2) corresponded with the SEM observations of the fungal hyphae. Only slight micromorphological changes were observed in Day 4 samples, corresponding to the decrease of polysaccharide abundance in molecular analyses (Fig. 1), likely because the process of fungal biomass degradation requires time to degrade complex compounds into more digestible sugars and because the plant leaf cuticular membrane is an efficient microbe invasion barrier, with the only ports of entry the stomata through which fungus can grow and excrete degradative enzymes. After fungal hyphae successfully penetrate stomata and start in situ decomposition of leaf tissue, initial fungal growth is slow due to limited hyphal tips from which new hyphae are developed (Trinci, 1972; Prosser and Trinci, 1978; Bartnicki-Garcia et al., 2000), as detected on Day 9 samples (e.g., Plate II, 4). Once a critical mass of hyphae has accumulated, the fungi grow exponentially and rapidly occupy the whole leaf interior space by Day 21 and 25 (e.g., Plate II, 8), consequently causing the rapid increase in polysaccharide abundance.

We suggest that the initial decline indicates the breakdown of the polysaccharides in the leaf and the latter increase indicates the consumption of those breakdown products, fungal hyphal growth, and the buildup of polysaccharide-rich fungal cell walls. Because the leaf and fungi are not readily separated once the hyphae have fully penetrated the inner leaf, the polysaccharide contents of both leaf and fungi are measured together. Interestingly, the total polysaccharide abundance between the first and last laboratory decay samples is negligible despite the drastic tissue decay seen in leaf micromorphology, suggesting that the carbon in the system was completely recycled. This supports the concept of plant material loss and recycling by microbial biomass that has been suggested by degradation studies conducted on other plant species, including lignin and polysaccharides (Opsahl and Benner, 1995), as well as amino acids and proteins (Hicks et al., 1991).

Because we observed very similar degradation patterns between the laboratory decay series and the natural decay series via SEM (Plate I), we propose that the main difference between the perceived organic geochemical results is whether the experiment is an opened or closed system. The laboratory decay series is confined entirely to the petri dish, making the entire carbon system closed between the leaf and fungi. In the natural decay series, however, the open-air leaves (M-M-83-B1 to B4) have less contact with microbial communities and thus show less degradation. Once the leaves land in the pond, the leaves then rapidly degrade in the open aquatic system via microbial, hydrological, and other degradation processes, leading to leaching as observed in previous aquatic plant decomposition studies (e.g. Valiela et al., 1985; Opsahl and Benner, 1995). It is also worth noting that the natural decay series would experience a consortium of microbes in competition with each other in the environment, which would be very hard to replicate in a laboratory environment.

The changes in polysaccharide contents during plant degradation emphasizes the significance of cross-referencing multiple methodologies in experimental taphonomy studies (Briggs et al., 2016; Briggs and McMahon, 2016), e.g. both morphological and organic geochemical together.

4.2. Molecular basis for the preservation of three-dimensional morphology

To better understand the molecular basis for the preservation of three-dimensional morphology of plant cells, we focus our discussion on the vascular bundle and adjacent areas where all cell wall structural biomolecules can be found (Plate I). Following the microbial removal of polysaccharides in the laboratory decay series, we observed a progressive collapse of cell walls which maintain the structural integrity of *Metasequoia* leaf cells (Plate I, 1–4). As expected, we observed that most cells in the phloem collapse earlier than tracheids in the xylem and transfusion tissues. Day 9 samples show the turning point in the molecular (Fig. 1) and morphological degradation (Plate I, 2) and this coincides with when the fungal hyphae are first seen entering the interior of the leaf (Plate II, 4). Via direct endocellulases by *G. candidum*, the partial removal of polysaccharides in the middle lamella and primary walls results in radically decreased support to the unevenly deposited secondary cell walls (Plate II, 3). Although partially detached, the secondary cell walls are still rigid, indicating the persistence of their original structural molecules, mainly lignin-strengthened cellulose. However, by Day 21, there is an obvious unraveling of the secondary cell walls from the tracheids (Plate II, 6–7). The string-like ravels indicate that the lignin-strengthened polysaccharides in the secondary cell walls are indeed more resistant to polysaccharide-degrading microbes. In Day 25 samples, some tracheids may still maintain their three-dimensional shape solely by their secondary cell walls which are loosened and readily collapsed; overall, most cells have collapsed (Plate I, 4). This supports the observations that suggest molecular degradation in gymnosperm and angiosperm woods include the rapid removal of hemicellulose, followed by the gradual removal of cellulose, and then the gradual modification of lignin (Hedges et al., 1985; Stout et al., 1988).

Our SEM observations confirm that the preservation of three-dimensional structure of a leaf is mainly due to the rigidity of cell walls. Along with the degradation of molecules in the middle lamella, then the primary cell wall, and finally the secondary cell wall, parenchyma cells (such as leaf mesophyll cells and phloem cells) collapse first and cells with secondary cell walls (such as tracheids in xylem and transfusion tissues) maintain their three-dimensional structures until the polysaccharides in the secondary cell walls are decomposed by e.g., laccases to degrade lignin by microbes much later.

4.3. Characteristics of modern leaves compared with fossil counterparts

Both the modern and extraordinarily-preserved fossil *Metasequoia* leaves possess similar molecular characteristics, containing the same diverse suite of polysaccharide pyrolysates (Yang et al., 2005; Gupta et al., 2009). The abundance of polysaccharide moieties in fossil *Metasequoia* does not correlate with the age of the fossil but instead correlates with morphological preservation, in accordance with the literature that inspired the current study (Yang et al., 2005; Witkowski et al., 2012). For example, despite being the oldest sample in this study, the Paleocene leaves (M-P-15, ca. 60 Ma) display the best molecular preservation with the most preserved polysaccharides in the highest abundances. The Eocene leaves (M-E-10, ca. 45 Ma) also maintain most of their major polysaccharides. The Miocene leaves (M-C-11, ca. 15 Ma) have only three detectable polysaccharide pyrolysate markers with much lower abundances than the other fossil leaves (for details see Yang et al., 2005).

The depositional environment for these three distinct sites are proposed to have been terrestrial aquatic environments, likely standing water with anoxic bottom waters, and experienced rapid organic matter burial. The Paleocene leaves were likely deposited in a floodplain or swamp (McIver and Basinger, 1999). The Eocene leaves were likely deposited in poorly drained floodplain forest; Schoenhut et al. (2004) shows that the pH of the standing water may have been very basic, maintained by a natural carbonate buffering system, which helped preserve these exceptional fossils. The Miocene leaves from Clarkia were deposited in the unoxidized zone of a lake with accumulation rates of ~12 mm/yr, considered very high accumulation for a stratified lake (Zolitschka et al., 2015) with acidic conditions (Schoenhut et al., 2004), possibly due to the proximal volcanism to the Clarkia site.

Proposed conditions for preventing organic matter decay and the formation of *Lagerstätte* include 1) high sedimentation rates for quick burial, 2) low oxygen concentrations, 3) cold water temperatures, 4) low light conditions, and 5) very acidic or very basic water chemistry (e.g. Sanger, 1986; Schoenhut, 2005; Schoenhut et al., 2004). In particular, the rapid burial of organic matter in stratified lakes has been

considered the critical controlling factor for the exceptional preservation of organic fossils (Seilacher et al., 1985; Briggs, 2003), which these three fossil depositional environments from Paleocene, Eocene, and Miocene appear to have had. These three sites also appear to have had low oxygen depositional conditions. Low light conditions were likely present at the two high latitude Arctic sites (i.e. the Paleocene Ellesmere Island and Eocene Axel Heiberg Island) but unlikely at the Miocene Clarkia site; this may explain why the fossil leaves from the two Arctic sites were slightly better preserved than the Clarkia site. Cold water temperatures were unlikely at any of the three sites given the hothouse and warmhouse climates experienced during the geologic times when the fossil leaves were deposited (e.g. Westerhold, 2020). Regarding the water chemistry, there is no clear evidence for the pH values at the Paleocene depositional environment (although there may have been acidic conditions given that this was possibly a swamp), there were possibly very basic pH values at the Eocene site, and there were possibly very acidic conditions at the Miocene site.

Thus, in context of the literature and given that the molecular analyses of these *Metasequoia* fossils show only partial removal of polysaccharides with virtually no reduction of resistant macromolecules such as lignin, we postulate that the important factors for the formation of these plant fossil *Lagerstätten* were indeed rapid burial and low oxygen conditions that prevented microbial degradation.

Although the overall molecular and morphological characteristics between modern and fossil *Metasequoia* leaves remain constant, the $\delta^{13}C$ values of bulk leaf tissues from fossil *Metasequoia* leaves are notably 4‰ more negative than their modern counterparts. In both modern decay series, the $\delta^{13}C$ values of bulk leaf vary little over the course of degradation, remaining relatively stable around −28‰. In the closed-system laboratory decay series, the $\delta^{13}C$ of the bulk tissues remains constant as microbes reincorporate leaf carbon into their bodies (Fig. 2). In the open natural decay series, minimal isotopic change of ca. 1‰ was observed during senescence and early diagenesis due to the removal of polysaccharides from plant tissues (note analytical instrumentation is ±0.5‰). The observation in both modern decay series is consistent with reports by Schweitzer et al. (1999) in which grasses and legumes were decayed for 119 days and by Nguyen Tu et al. (2004) on *Ginkgo* leaves through senescence and early diagenesis; when all reactants are consumed and converted to products in an irreversible open system, little carbon isotope fractionation occurs during the process.

Likewise, the $\delta^{13}C$ values of *n*-alkanes from fossil *Metasequoia* leaves are also 4‰ more positive than their modern counterparts (Fig. 2). Our results from the natural decay series show minimal change over time; the $\delta^{13}C$ values for each *n*-alkane chain-length nearly all fall within one standard deviation and all within two standard deviations (Fig. 3). For C_{29} and C_{31} *n*-alkanes, two standard deviations from the mean (±0.6‰ and ± 0.4‰, respectively) are in line with the ±0.5‰ error associated with the analytical instrumentation, further emphasizing the minimal variation among samples. Collister et al. (1994) have likewise observed small variations in isotopic values among individual compounds and emphasize caution in interpreting this minor variation as reflecting a signal change. Thus, our modern natural decay series shows a lack of isotopic change, supporting previous studies (e.g., Huang et al., 1995; Huang et al., 1997; Li et al., 2017) which have suggested that early stages of diagenesis cause little isotopic fractionation and that molecular carbon isotope signals of *n*-alkanes are stable and consequently reliable proxies.

As a result, we believe that the positive isotope shift seen in these exceptionally-preserved Cenozoic *Metasequoia* fossils (ca. 4‰ in comparison with its modern counterparts) is not likely caused by isotope fractionation associated with microbial decay or early diagenesis. Rather, they reflect the original plant physiology and environmental conditions registered as stable carbon isotope signals in these *Metasequoia* leaves.

Leaf-based paleo-CO_2 proxies, such as gas exchange models (Konrad et al., 2008, 2017; Franks et al., 2014) or the $\Delta^{13}C$ method based on the empirical relationship between changes of net carbon isotope fractionation of C_3 plants (Schubert and Jahren, 2012; Cui and Schubert, 2016) require bulk-leaf carbon isotope composition as a key parameter or the sole data for ancient CO_2 reconstruction. Recent plant growth chamber experiments with careful control of moisture availability and relative humidity show a strong response of plant ^{13}C fractionations to varying pCO_2 levels, suggesting that the plant tissue $\delta^{13}C$ values might be used as a paleo-CO_2 proxy (Schubert and Jahren, 2012, 2015; Cui and Schubert, 2016). The accuracy of these leaf-based pCO_2 proxies requires primary $\delta^{13}C$ signatures obtained from fossil plant tissues with minimal senescence and diagenesis impacts, or alternatively, a systematic bias of $\delta^{13}C$ values shift during fossilization can be detected, evaluated, and corrected. If the process leading to systematic shifts of bulk leaf $\delta^{13}C$ values is better known, corrections can be made to ensure the accuracy of model outcomes (Liang et al., 2022). Our experiments of two decay series confirmed that both senescence and early degradation alter ^{13}C fractionation very little, confirming the potential of using material from plant fossil *Lagerstätten* for the leaf-^{13}C pCO_2 proxy. Certainly, due to the limited time span of our two experiments concerning only early decay and early diagenesis, we recommend using fossil *Lagerstätte* materials such as the three-dimensionally-preserved Cenozoic *Metasequoia*, *Pseudolarix*, and *Larix* from Canadian Arctic areas (Yang et al., 2005). These fossil remains have great advantages over no*n-Lagerstätte* fossils whose isotope fidelity might have been compromised by decay and diagenesis. Along with that plant ^{13}C fractionation has not drastically changed over time due to evolution (Diefendorf et al., 2015), the conservative nature of these exceptionally-preserved Cenozoic conifers in fossil *Lagerstätten* are ideal candidates to be used for the reconstruction of geological pCO_2 using the new leaf-^{13}C pCO_2 proxy.

5. Conclusions

We conducted degradation experiments for *Metasequoia* leaves in two decay series: in a closed laboratory-controlled environment and in an open natural decay time sequence. We documented molecular, morphologic, and carbon isotopic changes for the leaves during these degradation processes. Through the laboratory decay series, fungal decomposition is observed; we suspect that the secretion of exocellulase (i.e., extracellular digestive enzyme) passes through stomata to break down leaf biomolecules (Barr et al., 1996). This initial attack is followed by the invasion of fungal hyphae through stomata into the leaf interior, leading to the final in situ decay which exponentially remove leaf polysaccharides. We confirmed the high efficiency of microbes to degrade leaf polysaccharides, as seen by the similar polysaccharide abundances at the beginning and ending points of the laboratory decay experiment, and the similar isotopic values throughout both decay series. In both decay series, we observed that the removal of polysaccharides directly relates to the decomposition of micromorphological features in the leaf, confirming the previous observations that polysaccharides might have played a critical role in preserving three-dimensional cellular structures in plant fossil leaves based upon limited fossil materials.

Our comparison between modern and Cenozoic *Metasequoia* leaves show similar leaf structural features and molecular features, confirming the evolutionary stasis of this genus and the halt of decay at the early stages for these fossil *Lagerstätten*, substantiating the promise of using these plant fossils as a paleoenvironmental proxy. Because the stable carbon isotope analysis in modern leaves show no or little fractionation in $\delta^{13}C$ values during the early degradation processes, the ca. 4‰ positive shift in $\delta^{13}C$ of fossil *Metasequoia* from fossil *Lagerstätten* is not likely due to decay nor different physiology, but instead to the change of environment and/or climate. Given the recent development of using $\delta^{13}C$ values from plant material as a proxy or employing $\delta^{13}C$ values as a key parameter for reconstructing ancient pCO_2 (e.g., Schubert and Jahren, 2012, 2015; Diefendorf et al., 2010, 2015; Cui and Schubert,

2016; Franks et al., 2014; Liang et al., 2022), our study provides a timely critique for the evaluation of its carbon isotopic fidelity.

Declaration of Competing Interest

The authors declare that they have no known competing financial interests or personal relationships that could have appeared to influence the work reported in this paper.

Acknowledgements

We thank Christopher Williams for providing Canadian Arctic fossil samples, Gerard Olack (Yale University) and Weiguo Liu (Chinese Academy of Sciences) for carbon isotope analysis, and Hongmei Wang (China University of Geoscience at Wuhan) for the use of her laboratory for microbial degradation. CRW was supported by a HanBan Scholarship for her one-year study at China University of Geoscience in Wuhan.

References

Anthon, G.E., Barrett, D.M., 2001. Colorimetric method for the determination of lipoxygenase activity. J. Agric. Food Chem. 49 (1), 32–37.

Bajpai, V.K., Rahman, A., Kang, S.C., 2007. Chemical composition and anti-fungal properties of the essential oil and crude extracts of *Metasequoia glyptostroboides* Miki ex Hu. Ind. Crop. Prod. 26, 28–35.

Barclay, R.S., Wing, S.L., 2016. Improving the Ginkgo CO_2 barometer: implications for the early Cenozoic atmosphere. Earth Planet. Sci. Lett. 439, 158–171.

Barr, B.K., Hseih, Y.-L., Ganem, B., Wilson, D.B., 1996. Identification of two functionally different classes of exocellulases. Biochemistry. 35 (2), 586–592.

Bartnicki-Garcia, S., Bracker, C.E., Gierz, G., Lopez-Franco, R., Lu, H., 2000. Mapping the growth of fungal hyphae: orthogonal cell wall expansion during tip growth and the role of turgor. Biophys. J. 79 (5), 2382–2390.

Blanchette, R.A., Cease, K.R., Abad, A., Burnes, T., 1991. Ultrastructural characterization of wood from Tertiary fossil forest in the Canadian Arctic. Can. J. Bot. 69, 560–568.

Briggs, D.E.G., 2003. The role of decay and mineralization in the preservation of soft-bodied fossils. Annu. Rev. Earth Planet. Sci. 31, 275–301.

Briggs, D.E.G., McMahon, S., 2016. The role of experiments in investigating the taphonomy of exceptional preservation. Palaeontology 59, 1–11. https://doi.org/10.1111/pala.12219.

Briggs, D.E.G., Gupta, N.S., Cambra-Moo, O., 2016. Molecular preservation. In: Poyato-Ariza, F.J., Buscalioni, A.D. (Eds.), Las Hoyas: A Cretaceous wetland. A multidisciplinary synthesis after 25 years of research on an exceptional fossil *Lagerstätte* from Spain, pp. 216–219.

Butrim, M.J., Royer, D.L., 2020. Leaf-economic strategies across the Eocene–Oligocene transition correlate with dry season precipitation and paleoelevation. Am. J. Bot. 107 (12), 1772–1785.

Chikaraishi, Y., Naraoka, H., 2003. Compound-specific δD–δ^{13}C analyses of *n*-alkanes extracted from terrestrial and aquatic plants. Phytochemistry 63, 361–367.

Collister, J., Rieley, G., Stern, B., Eglinton, G., Fry, B., 1994. Compound-specific δ^{13}C analyses of leaf lipids from plants with differing carbon dioxide metabolisms. Org. Geochem. 21, 619–627.

Cui, Y., Schubert, B.A., 2016. Quantifying uncertainty of past pCO_2 determined from changes in C_3 plant carbon isotope fractionation. Geochim. Cosmochim. Acta 172, 127–138.

Diefendorf, A.F., Mueller, K.E., Wing, S.L., Kock, P.L., Freeman, K.H., 2010. Global patterns in leaf ^{13}C discrimination and implications for studies of past and future climate. Proc. Natl. Acad. Sci. 107 (13), 5738–5743.

Diefendorf, A.F., Freeman, K.H., Wing, S.L., Currano, E.D., Mueller, K.E., 2015. Paleogene plants fractionated carbon isotopes similar to modern plants. Earth Planet. Sci. Lett. 429, 33–44.

Eberle, J.J., Storer, J.E., 1999. Northernmost record of brontotheres, Axel Heiberg Island, Canada – Implications for age of the Buchanan Lake Formation and brontothere paleobiology. J. Paleontol. 73, 979–983.

Eliskases-Lechner, F., Guéguen, M., Panoff, J.M., 2022. Geotrichum candidum. In: McSweeney, P.L.H., McNamara, J.P. (Eds.), Encyclopedia of Dairy Sciences (Third edition). Academic Press, pp. 561–568.

Franks, P.J., Royer, D.L., Beerling, D.J., Van de Water, P.K., Cantrill, D.J., Barbour, M.M., Berry, J.A., 2014. New constraints on atmospheric CO_2 concentration for the Phanerozoic. Geophys. Res. Lett. 41, 4685–4694.

Gupta, N.S., Yang, H., Leng, Q., Briggs, D.E.G., Cody, G.E., Summons, R.E., 2009. Diagenesis of plant biopolymers: decay and macromolecular preservation of *M. glyptostroboides*. Org. Geochem. 40, 802–809.

Hedges, J.I., Cowie, G.L., Ertel, J.R., Barbour, J.R., Hatcher, P.G., 1985. Degradation of carbohydrates and lignins in buried woods. Geochim. Cosmochim. Acta 49, 701–711.

Hicks, R.E., Lee, C., Marinucci, A.C., 1991. Loss and recycling of amino acids and protein from smooth cordgrass (*Spartina alterniflora*) litter. Estuaries. 14, 430–439.

Höfig, D., Zhang, Y.-G., Giosan, L., Leng, Q., Liang, J.-Q., Wu, M.-X., Miller, B.V., Yang, H., 2021. Annually-resolved sediments in the classic Clarkia lacustrine deposits during the middle Miocene Climatic Optimum. Geology 49, 916–920.

Huang, Y., Lockheart, M., Collister, J.W., Eglinton, G., 1995. Molecular and isotopic biogeochemistry of the Miocene Clarkia Formation: hydrocarbons and alcohols. Org. Geochem. 23, 785–801.

Huang, Y., Eglinton, G., Ineson, P., Latter, P.M., Bol, R., Douglas, D.D., 1997. Absence of carbon isotope fractionation of individual *n*-alkanes in a 23-year field decomposition experiment with *Calluna vulgaris*. Org. Geochem. 26, 497–501.

Konrad, W., Roth-Nebelsick, A., Grein, M., 2008. Modelling of stomatal density response to atmospheric CO_2. J. Theor. Biol. 253, 638–658.

Konrad, W., Katul, G., Roth-Nebelsick, A., Grein, M., 2017. A reduced order model to analytically infer atmospheric CO_2 concentration from stomatal and climate data. Adv. Water Resour. 104, 145–157.

Lallier-Vergès, E., Marchand, C., Disnara, J.-R., Lottiera, N., 2008. Origin and diagenesis of lignin and carbohydrates in mangrove sediments of Guadeloupe (French West Indies): evidence for a two-step evolution of organic deposits. Chem. Geol. 255, 388–398.

Leng, Q., Yang, H., Yang, Q., Zhou, J., 2001. Variation of cuticle micromorphology of *M. glyptostroboides* (Taxodiaceae). Bot. J. Linn. Soc. 136 (2), 207–219.

Leng, Q., Langlois, G.A., Yang, H., 2010. Early Paleogene Arctic terrestrial ecosystems affected by the change of polar hydrology under global warming: Implications for modern climate change at high latitudes. Sci. China Earth Sci. 53 (7), 933–944.

LePage, B.A., Yang, H., Matsumoto, M., 2005. The evolution and biogeographic history of *Metasequoia*. In: LePage, B.A., Williams, C.J., Yang, H. (Eds.), The Geobiology and Ecology of *Metasequoia*. Topics in Geobiology. Springer Netherlands Dordrecht, the Netherlands, Norwell, MA, USA, pp. 3–114.

Li, C., Yang, Q., 2003a. Polymorphism of ITS sequences of nuclear ribosomal DNA in *Metasequoia glyptostroboides*. J. Genet. Mol. Biol. 13, 264–271.

Li, C., Yang, Q., 2003b. Phylogenetic relationships among the genera of Taxodiaceae and Cupressaceae from 28S rDNA sequences. Hereditis 25, 177–180.

Li, R.-C., Fan, J., Xue, J.-T., Meyers, P.A., 2017. Effects of early diagenesis on molecular distributions and carbon isotopic compositions of leaf wax long chain biomarker n-alkanes: comparison of two one-year-long burial experiments. Org. Geochem. 104, 8–18.

Liang, M.M., Bruch, A., Collinson, M., Mosbrugger, V., Li, C.S., Sun, Q.G., Hilton, J., 2003. Testing the climatic estimates from different paleobotanical methods: an example from the Middle Miocene Shanwang flora of China. Palaeogeogr. Palaeoclimatol. Palaeoecol. 198 (3–4), 279–301.

Liang, J.-Q., Leng, Q., Höfig, D.F., Niu, G., Wang, L., Royer, D.L., Burke, K., Xiao, L., Zhang, Y.-G., Yang, H., 2022. Constraining conifer physiological parameters in leaf gas-exchange models for ancient CO_2 reconstruction. Global Planet. Change 209 Article number: 103737.

Liu, W., Ning, Y., An, Z., Wu, Z., Lu, H., Cao, Y., 2005. Carbon isotopic composition of modern soil and paleosol as a response to vegetation change on the Chinese Loess Plateau. Sci. China Ser. D Earth Sci. 48 (1), 93–99.

McIver, E.E., Basinger, J.F., 1999. Early Tertiary floral evolution in the Canadian high Arctic. Ann. Mo. Bot. Gard. 86, 523–545.

Nguyen Tu, T.T., Derenne, S., Largeau, C., Bardoux, G., Mariotti, A., 2004. Diagenesis effects on specific carbon isotope composition of plant *n*-alkanes. Org. Geochem. 35, 317–329.

Opsahl, S., Benner, R., 1995. Early diagenesis of vascular plant tissues: lignin and cutin decomposition and biogeochemical implications. Geochim. Cosmochim. Acta 59, 4889–4904.

Opsahl, S., Benner, R., 1999. Characterization of carbohydrates during early diagenesis of five vascular plant tissues. Org. Geochem. 30 (1), 83–94.

Pagani, M., Pedentchouk, N., Huber, M., Sluijis, A., Schouten, S., Brinkhuis, H., Sinninghe Damsté, J.S., Dickens, G.R., Expedition 302 Scientists, 2006. Arctic hydrology during global warming at the Palaeocene/Eocene thermal maximum. Nature. 442 (10), 671–675.

Polissar, P.J., Freeman, K.H., Rowley, D.B., McInerney, F.A., Currie, B.S., 2009. Paleoaltimetry of the Tibetan Plateau from D/H ratios of lipid biomarkers. Earth Planet Sci. Lett. 287 (1), 64–76.

Pouwels, A.D., Eijel, G.B., Boon, J.J., 1989. Curie-point pyrolysis-capillary gas chromatography-high resolution mass spectrometry of microcrystalline cellulose. J. Anal. Appl. Pyrolysis 14, 1426–1437.

Prosser, J.I., Trinci, A.P.J., 1978. A model for hyphal growth and branching. Microbiology. 111 (1), 153–164.

Sanger, J.E., 1986. Fossil pigments in paleoecology and paleolimnology. Palaeogeogr. Paleoclimatol. Paleoecol. 62, 343–359.

Schoenhut, K., 2005. Environmental implications of the preservation of chloroplast ultrastructure in Eocene *Metasequoia* leaves. Paleobiology. 31, 424–433.

Schoenhut, K., Vann, D.R., LePage, B.A., 2004. Cytological and ultrastructural preservation in Eocene *Metasequoia* leaves from the Canadian High Arctic. Am. J. Bot. 91, 816–824.

Schubert, B.A., Jahren, A.H., 2012. The effect of atmospheric CO2 concentration on carbon isotope fractionation in C3 land plants. Geochim. Cosmochim. Acta 96, 29–43.

Schubert, B.A., Jahren, A.H., 2015. Seasonal temperature and precipitation recorded in the intra-annual oxygen isotope pattern of meteoric water and tree-ring cellulose. Quat. Sci. Rev. 125, 1–14.

Schweitzer, M., Fear, J., Cadisch, G., 1999. Isotopic (δ^{13}C) fractionation during plant residue decomposition and its implications for soil organic matter studies. Rapid Commun. Mass Spectrom. 13, 1284–1290.

Seilacher, A., Reif, W.-E., Westphal, F., 1985. Sedimentological, ecological and temporal patterns of fossil *Lagerstätten*. Phil. Trans. R. Soc. Biol. Sci. 311, 5–24.

Spicer, R.A., Yang, J., Spicer, T.E.V., Farnsworth, A., 2021. Woody dicot leaf traits as a palaeoclimate proxy: 100 years of development and application. Palaeogeogr. Palaeoclimatol. Palaeoecol. 562 (15), 110138.

Stout, S.A., Boon, J.J., Spackman, W., 1988. Molecular aspects of the peatification and early coalification of angiosperm and gymnosperm woods. Geochim. Cosmochim. Acta 52, 405–414.
Trinci, A.P.J., 1972. A study of the kinetics of hyphal extension and branch initiation of fungal mycelia. Microbiology. 81 (1), 225–236.
Valiela, I., Teal, J.M., Allen, S.D., Van Etten, R., Goehringer, D., Volkman, S., 1985. Decomposition in salt marsh ecosystems: the phases and major factors affecting disappearance of above-ground organic matter. J. Exp. Mar. Biol. Ecol. 89, 29–54.
van Bergen, P.F., Collinson, M.E., DeLeeuw, J.W., 1996. Characterization of the insoluble constituents of propagule walls of fossil and extant water lilies: implication for the fossil record. Anc. Biomol. 1, 55–81.
van den Brink, J., de Vries, R.P., 2011. Fungal enzyme sets for plant polysaccharide degradation. Appl. Microbiol. Biotechnol. 91 (6), 1477–1492.
Wang, L., 2010. Morphology and anatomy of *M. glyptostroboides* leaves and their environmental indicative values: evidence from the comparative studies of "living fossil" and fossils. Nanjing Institute of Geology and Paleontology. The Graduate School of Chinese Academy of Sciences, Nanjing, p. 423.
Wei, H., Taylor, L.E., Baker, J.O., Tucker, M.P., Ding, S.-Y., 2009. Natural paradigms of plant cell wall degradation. Curr. Opin. Biotechnol. 20 (3), 330–338.
Westerhold, T., et al., 2020. An astronomically dated record of Earth's climate and its predictability over the last 66 million years. Science 369 (6509), 1383–1387.
Witkowski, C., Gupta, N.S., Yang, H., Leng, Q., Williams, C.J., Briggs, D.E.G., Summons, R.E., 2012. Molecular preservation of Cenozoic conifer fossil *Lagerstätten* from Banks Island, the Canadian Arctic. Palaios. 27 (5), 279–287.
Woodward, F.I., 1987. Stomatal numbers are sensitive to increases in CO_2 from pre-Industrial levels. Nature 327, 617–618.
Yang, H., 2005. Biomolecules from *Metasequoia*. In: LePage, B.A., Williams, C.J., Yang, H. (Eds.), The Geobiology and Ecology of *Metasequoia*. Springer, Dordrecht.
Yang, H., Huang, Y., 2003. Preservation of lipid hydrogen isotope ratios in Miocene lacustrine sediments and plant fossils at Clarkia, northern Idaho, USA. Org. Geochem. 34 (3), 413–423.
Yang, H., Jin, J.-H., 2000. Phytogeographic history and evolutionary stasis of *Metasequoia*: geological and genetic information contrasted. Acta Palaeontol. Sin. 39 (Supplements), 288–307.
Yang, H., Huang, Y., Leng, Q., LePage, B.A., Williams, C.J., 2005. Biomolecular preservation of Tertiary *M. glyptostroboides* fossil *Lagerstätten* revealed by comparative pyrolysis analysis. Rev. Palaeobot. Palynol 134 (3–4), 237–256.
Yang, H., Leng, Q., LePage, B.A., 2007. Labile biomolecules in three-dimensionally preserved early Tertiary *M. glyptostroboides* leaves from Ellesmere Island, Canada. Biological and geological applications. Bull. Peabody Mus. Nat. Hist. Yale Univ. 48, 317–328.
Yang, H., Pagani, M., Briggs, D.E.G., Equiza, M.A., Jagels, R., Leng, Q., LePage, B.A., 2009. Carbon and hydrogen isotope fractionation under continuous light: implications for paleoenvironmental interpretations of the High Arctic during Paleogene warming. Oecologia. 160, 461–470.
Yang, H., Blais, B.S., Leng, Q., 2011. Stable isotope variations from cultivated *Metasequoia* trees in the United States: a statistical approach to assess isotope signatures as climate signals. Jpn. Assoc. Hist. Bot. 19 (1–2), 75–88.
Zolitschka, B., Francus, P., Ojala, A.E.K., Schimmelmann, A., 2015. Varves in lake sediments—a review. Quat. Sci. Rev. 117, 1–41.